Article

Actin-Filament Stochastic Dynamics Mediated by ADF/Cofilin

Alphée Michelot,[1,5] Julien Berro,[2,5]
Christophe Guérin,[1] Rajaa Boujemaa-Paterski,[1]
Christopher J. Staiger,[3,4] Jean-Louis Martiel,[2,*]
and Laurent Blanchoin[1,*]

[1] Institut de Recherches en Technologie et Sciences
      pour le Vivant
Laboratoire de Physiologie Cellulaire Végétale
CEA Grenoble
Commissariat à l'Energie Atomique
Centre National de la Recherche Scientifique
Institut National de la Recherche Agronomique
Université Joseph Fourier
17 rue des Martyrs
F38054 Grenoble
France
[2] Laboratoire Techniques de l'Ingénierie Médicale
      et de la Complexité
Centre National de la Recherche Scientifique 5525
Pavillon Taillefer
Faculté de Médecine
F-38706 La Tronche
France
[3] Department of Biological Sciences and
[4] The Bindley Bioscience Center
Purdue University
West Lafayette, Indiana 47907-2064

Summary

Background: The rapid dynamics of actin filaments is a fundamental process that powers a large number of cellular functions. However, the basic mechanisms that control and coordinate such dynamics remain a central question in cell biology. To reach beyond simply defining the inventory of molecules that control actin dynamics and to understand how these proteins act synergistically to modulate filament turnover, we combined evanescent-wave microscopy with a biomimetic system and followed the behavior of single actin filaments in the presence of a physiologically relevant mixture of accessory proteins. This approach allows for the real-time visualization of actin polymerization and age-dependent filament severing.
Results: In the presence of actin-depolymerizing factor (ADF)/cofilin and profilin, actin filaments with a processive formin attached at their barbed ends were observed to oscillate between stochastic growth and shrinkage phases. Fragmentation of continuously growing actin filaments by ADF/cofilin is the key mechanism modulating the prominent and frequent shortening events. The net effect of continuous actin polymerization, driven by a processive formin that uses profilin-actin, and of

ADF/cofilin-mediating severing that trims the aged ends of the growing filaments is an up to 155-fold increase in the rate of actin-filament turnover in vitro in comparison to that of actin alone. Lateral contact between actin filaments dampens the dynamics and favors actin-cable formation. A kinetic simulation accurately validates these observations.
Conclusions: Our proposed mechanism for the control of actin dynamics is dominated by ADF/cofilin-mediated filament severing that induces a stochastic behavior upon individual actin filaments. When combined with a selection process that stabilizes filaments in bundles, this mechanism could account for the emergence and extension of actin-based structures in cells.

Introduction

Force generation lies at the heart of a large and diverse array of cellular processes, including morphogenesis, the establishment of polarity, and motility [1]. The actin cytoskeleton can produce these large forces directly based on three main properties: (1) the abundance of the major protein constituent, actin; (2) the potential to modulate polymerization and depolymerization with a battery of accessory proteins; and (3) the ability to self-organize into higher-order structures [2]. The basic unit in this system is monomeric actin, a 42 kDa protein that binds a nucleotide (ATP) and a divalent cation (Mg^{2+}). In vivo, MgATP-actin monomers assemble rapidly into polarized helical filaments that are a few microns in length and that make contacts with the plasma membrane to drive cell movement at rates of up to 10 μm/min [1]. To sustain movement over time and to be able to rapidly change the direction of movement in response to stimuli, locomoting cells need to continuously polymerize actin filaments at the leading edge and disassemble actin filaments at the rear of the lamellipodium. This fast actin-filament turnover has been established for several different cells, including fibroblasts [3], fish keratocytes [4], and neuronal growth cones [5]. Moreover, dynamic actin polymerization and depolymerization contribute to the formation of different actin-based structures, such as filopodia and microspikes [6], as well as yeast actin cables and patches [7]. However, the basic mechanisms underlying fast actin-filament turnover in vivo remain a central unanswered question in cell biology. Indeed, actin filaments in vitro are stable structures that turn over at rather slow rates by a mechanism called "treadmilling." At steady state, treadmilling comprises the addition of actin monomers at filament barbed ends and the accompanying depolymerization of actin subunits at filament pointed ends (rate of 0.27 s^{-1} [8]). This is two orders of magnitude too slow for it to be compatible with cell locomotion [9].

   Biomimetic systems that reconstitute actin-based motility in vitro are a valuable tool for identifying the minimum set of actin-binding proteins required for generating propulsion forces [10]. Here we use a combination of

*Correspondence: jean-louis.martiel@imag.fr (J.-L.M.), laurent.blanchoin@cea.fr (L.B.)
[5] These authors contributed equally to this work.
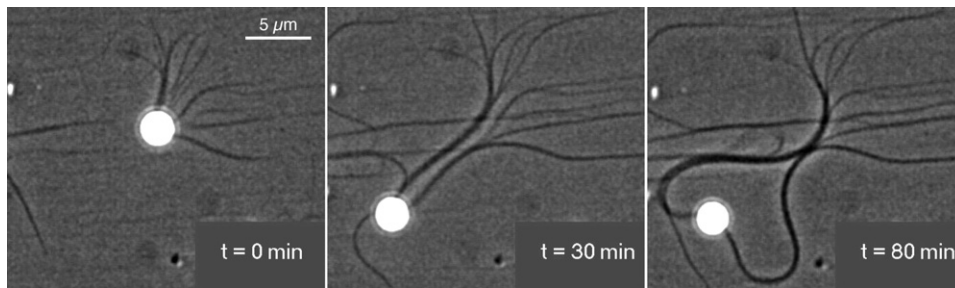
Figure 1. Motility of Polystyrene Beads Coated with the Formin mDia1 in a Biomimetic Reconstituted System

Conditions: mDia1-coated beads (1 μM) were added to a motility medium containing 8 μM F-actin, 4 μM profilin, and 10 μM human cofilin. Images were taken at the indicated times during polymerization.

Time-lapse images of motile mDia1 beads were acquired by phase-contrast microscopy. After a few minutes, actin-filament cables appeared and managed to propel the bead, in this representative example. If any obstacle stopped the bead, the force from actin polymerization buckled the actin cables instead of pushing the bead (t = 80 min). See also Movie S1. The scale bar represents 5 μm.

such a system and total-internal-reflection fluorescence microscopy (TIRFM), which allows for the direct visualization of single actin filaments and the characterization of the molecular mechanism underlying physiological actin-filament turnover. In this system, individual actin filaments attached to a polystyrene bead with a processive formin revealed a highly dynamic behavior in which continuous growth alternates with catastrophic reductions in overall filament length. We find that the severing activity of actin-depolymerizing factor (ADF)/cofilin plays a central role in this stochastic actin-filament-length oscillation by trimming the aged end of a filament that continues to grow at the barbed end. Lateral interactions between actin filaments modulate filament stability and are essential for actin-cable formation and bead motility. Based on experimental parameters, we have developed a kinetic model that validates our observations.

Results

Actin Polymerization at the Surface of Formin-Coated Beads Generates Motility

Polystyrene beads coated with the actin-promoting factor of formin, mDia1 FH1-FH2, were added to a mixture of purified proteins, including actin filaments, profilin, and ADF/cofilin. Actin polymerization was initiated from their surface, and ultimately bead movement could be observed at a velocity of 0.2 μm · min⁻¹ by phase-contrast microscopy (Figure 1 and [11]). A "tail" of actin filaments attached to the bead comprises two large actin-filament bundles that are arrayed at 180° from each other (Figure 1; Movie S1 in the Supplemental Data available online). We hypothesize that movement reflects the continuous insertional polymerization of actin filaments due to a processive nucleation–elongation factor (i.e., the formin mDia1) at the surface of the bead and the actin-filament shortening induced by ADF/cofilin. When the bead stops moving, due to nonspecific interactions with other filament bundles in the mixture or with the cover glass, actin polymerization continues and is powerful enough to buckle actin-filament bundles (Figure 1, t = 80 min; Movie S1). Such buckling events have also been observed for individual actin filaments constrained in space by mDia1 attached to the growing barbed ends and by NEM-myosin II attached to the filament side [12, 13].

Direct Visualization of Individual Actin-Filament Polymerization at the Surface of mDia1-FH1-FH2-Coated Beads

We used TIRFM to follow the nucleation and polymerization of single actin filaments at the surface of beads coated with mDia1 FH1-FH2 (Figure 2A; Movies S2–S6). An advantage of our experimental design compared to those of previous TIRFM experiments with formins is that we know the exact location of mDia1 (i.e., at the bead surface). We introduced mDia1-coated beads into a TIRFM flow chamber and initiated polymerization by adding rhodamine- or Alexa-532-labeled actin monomers, initially in the presence of an excess of profilin (Figure 2A; Movies S2–S4). A few seconds after the addition of profilin-actin, actin filaments nucleated from the surface of the bead by mDia1 grew continuously at a rate of up to $k_+ = 38 \ \mu M^{-1} \cdot s^{-1}$ (Figures 2A and 2C; Movies S2–S4), in agreement with previous reports [13, 14]. We were able to modulate the density of actin filaments generated at the surface of the beads by varying the concentration of attached formins (compare Movies S2 and S3). We obtained a linear correlation between the concentration of attached mDia and the efficiency of actin-filament nucleation from the beads (data not shown).

We recently established that Alexa-532 actin is a useful tool for identifying and following polymerization at the growing barbed end of actin filaments [13]. The intensity of Alexa-532-actin-filament fluorescence decreases rapidly as a result of photobleaching, with the result that subunits near the growing barbed ends are substantially brighter than older parts of the filament [13]. This decrease is not related to the loss of fluorescence when an actin filament moves out of the evanescent wave; indeed, comparable bleaching is not observed with rhodamine-labeled actin. By using Alexa-532 actin, we demonstrated here that mDia1 attached to the beads is processive (Movie S4). The brightest part of an actin filament, corresponding to the growing barbed end, was always in contact with the formin attached to the beads (green arrows, Movie S4), whereas fluorescence of the actin filament near the pointed end decreased markedly over time (blue arrows, Movie S4). When actin filaments that initiated at the bead surface came into contact with the glass slide, we often observed buckling events, consistent with the processive behavior of mDia1 (Figure 2A; Movies S2–S4).
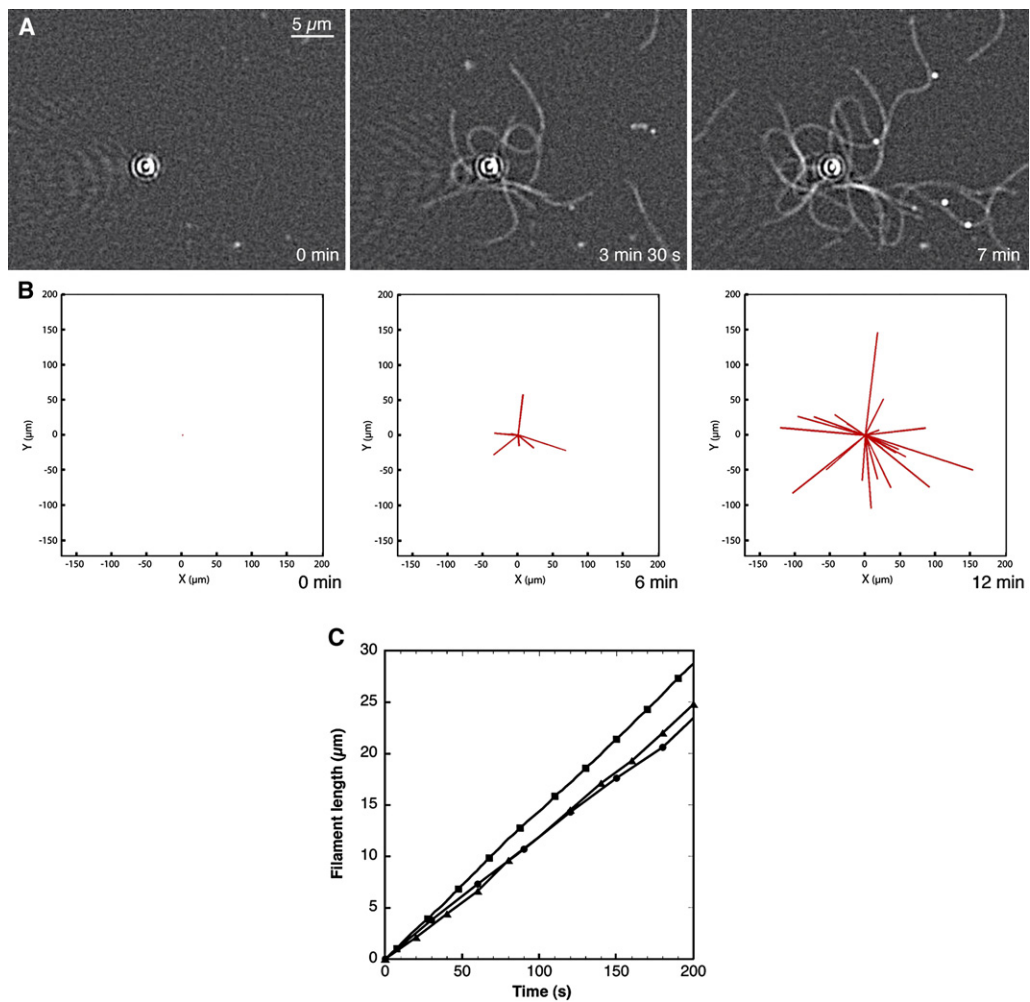
Figure 2. TIRF Microscopy is a Powerful Tool for the Visualization of Individual Actin Filaments Polymerizing at the Surface of mDia1-Coated Beads

Conditions: mDia1-coated beads (100 nM) were attached to the cover glass before the addition of 1.2 μM rhodamine-labeled actin monomers in the presence of 3.6 μM profilin.

(A) Time-lapse evanescent-wave microscopy of rhodamine-labeled-actin polymerization around 100 nM mDia1-coated beads (corresponding to 12 molecules of active mDia1 per μm^2, on average). Almost all filaments were nucleated from the beads and remained attached while elongating. Actin filaments under these conditions grew at a rate of $k_+ = 38\ \mu M^{-1} \cdot s^{-1}$. Moreover, filaments nucleated from the beads often buckled, as expected for a processive elongation factor. See also Movie S2.

(B) In silico modeling of the polymerization of 1.2 μM actin around 100 nM mDia1-coated beads. Actin filaments are represented as red sticks centered on the central position where the bead remains. Actin filaments elongated progressively as long as polymerization occured. See also Movie S7.

(C) The length of an actin filament over time as monitored by TIRFM, for a rhodamine labeled (circles) or an Alexa-532 labeled (triangles) filament, is compared with the in silico growth of an actin filament (squares). At this point in the experiment, filaments elongated linearly over time and grew at a fast rate (i.e., 38 $\mu M^{-1} \cdot s^{-1}$), consistent with the unique properties of mDia1 in the presence of profilin.

Whether profilin is necessary for the processive behavior of mDia1 remains controversial [11, 14]. However, we were able to induce growth of actin filaments, at a rate of $k_+ = 7.8\ \mu M^{-1} \cdot s^{-1}$, from the surface of mDia1-coated beads in the absence of profilin (Movies S5 and S6). Moreover, the use of Alexa-532-actin allowed us to show that the growing barbed end was continuously attached to a formin at the surface of a bead (green arrow, Movie S6). These observations, and the fact that actin filaments initiated from the bead surface often buckle (Movie S6), demonstrate that profilin is not necessary for formin processivity and are in agreement with Kovar et al. [14].

To simulate the nucleation and growth of actin filaments during evanescent-wave-microscopy experiments, we developed a 2D kinetic model (see Experimental Procedures and Figures S1 and S2) that accounts for the full process of nucleation and processive elongation at the surface of a bead (Figures 2B and 2C; Movie S7). The model addresses only the kinetics of filament growth; as a consequence, we neglected all filament-shape fluctuations (see Supplemental Data for a discussion of this hypothesis). The rate of elongation and the density of actin filaments generated at the surface of the beads agreed between experimental and simulated data (Figure 2C).
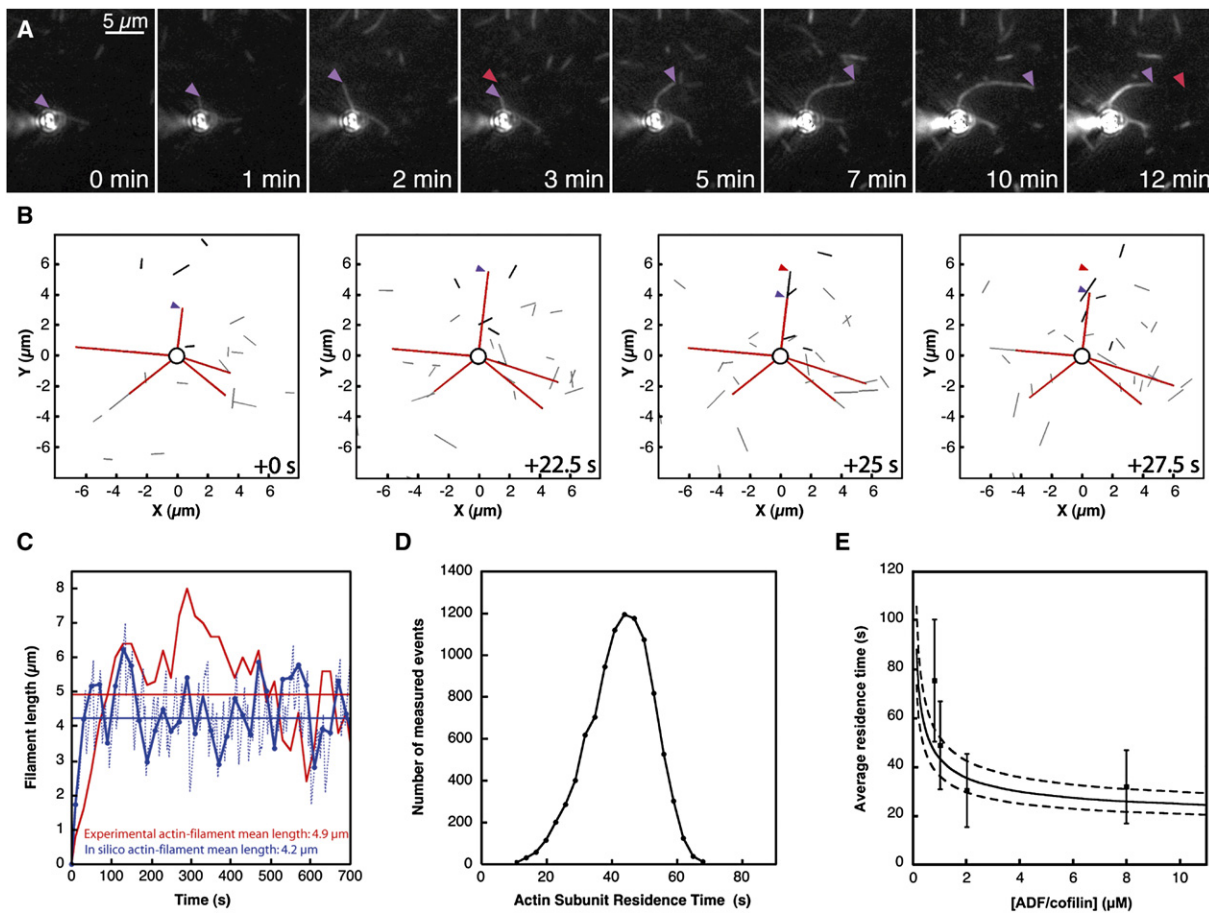
Figure 3. A Reconstituted System with Formin, Profilin, and ADF/Cofilin Induces a Stochastic Behavior of Growing Actin Filaments and Accelerates Their Turnover

Conditions: mDia1-coated beads (100 nM) were attached to the cover glass before the addition of 1.2 μM rhodamine-labeled actin monomers in the presence of 3.6 μM profilin and 1 μM human cofilin. Purple arrows follow the actin-filament end during elongation, whereas the red arrows represent the last observed position of a filament end before shortening.

(A) Time-lapse evanescent-wave microscopy of rhodamine-labeled-actin polymerization around mDia1-coated beads in the presence of human cofilin and profilin. Human cofilin severed actin filaments while they elongated, thereby accelerating the turnover of actin subunits through the filament pool that remained attached to the beads. See also Movie S8.

(B) In silico modeling of actin polymerization around 100 nM mDia1-coated beads in the presence of 1 μM human cofilin and 3.6 μM profilin. Red sticks representing actin filaments around mDia1-coated beads show a stochastic dynamic behavior due to the synergistic effects of formin, profilin, and ADF/cofilin. See also Movie S10.

(C) Length fluctuations of an actin filament over time for experimental data (red curve) and for a representative example of in silico data (blue dotted curve). Blue dots represent the length of the in silico actin filament every 20 s (corresponding to the sampling time of the camera during TIRFM experiments). The theoretical blue curve links the blue dots and predicts the length variation that might be observed experimentally. Straight lines represent the average length both experimentally (red line) and in silico (blue line).

(D) Distribution of subunit residence time obtained from in silico reconstitution of actin-filament turnover in the presence of formin, profilin, and ADF/cofilin. The residence time peaks at approximately 43 s. (average ± SD ~43 ± 9.7 s) and is limited either by the time delay for the P_i dissociation (distribution lower limit, ~10 s) or by the binding of ADF/cofilin to the actin filament (distribution upper limit, ~65 s). All actin subunits in a filament are replaced after a time interval of about 65 s, the maximal time residence obtained from simulations. See also Movie S11.

(E) Average residence time of subunits in actin filaments in the presence of ADF/cofilin. Error bars represent variability in measurements.

Both experiments (filled circles) and simulations (solid line) show that the subunit residence time is extremely sensitive to the presence of ADF/cofilin at a low concentration (below 1 μM). This residence time is bounded at high ADF/cofilin concentrations by a lower value, about 25 s. Simulations were carried out with the conditions of Figure 3D (dotted lines and vertical bars indicate the variance for simulated and experimental data, respectively).

Synergistic Effects of Formin, Profilin, and ADF/Cofilin Induce Stochastic Growth and Shortening, Resulting in Rapid Turnover of Growing Actin Filaments

We next reconstituted single-actin-filament dynamics by introducing mDia1-coated beads into the flow chamber and then added rhodamine-actin monomers, profilin, and ADF/cofilin (Figures 3A and 4A; Movies S8 and S12). A few seconds after the addition of the protein mixture, actin filaments were initiated at the surface of the bead (Figure 3A). Initially, these filaments grew continuously at a rate of up to 38 $μM^{-1} \cdot s^{-1}$. However, after the initial period, these actin filaments were observed to switch rapidly between phases of elongation (Figure 3A, purple triangle; Movie S8) and shortening (Figure 3A, red triangle; Movie S8). This is remarkable because until
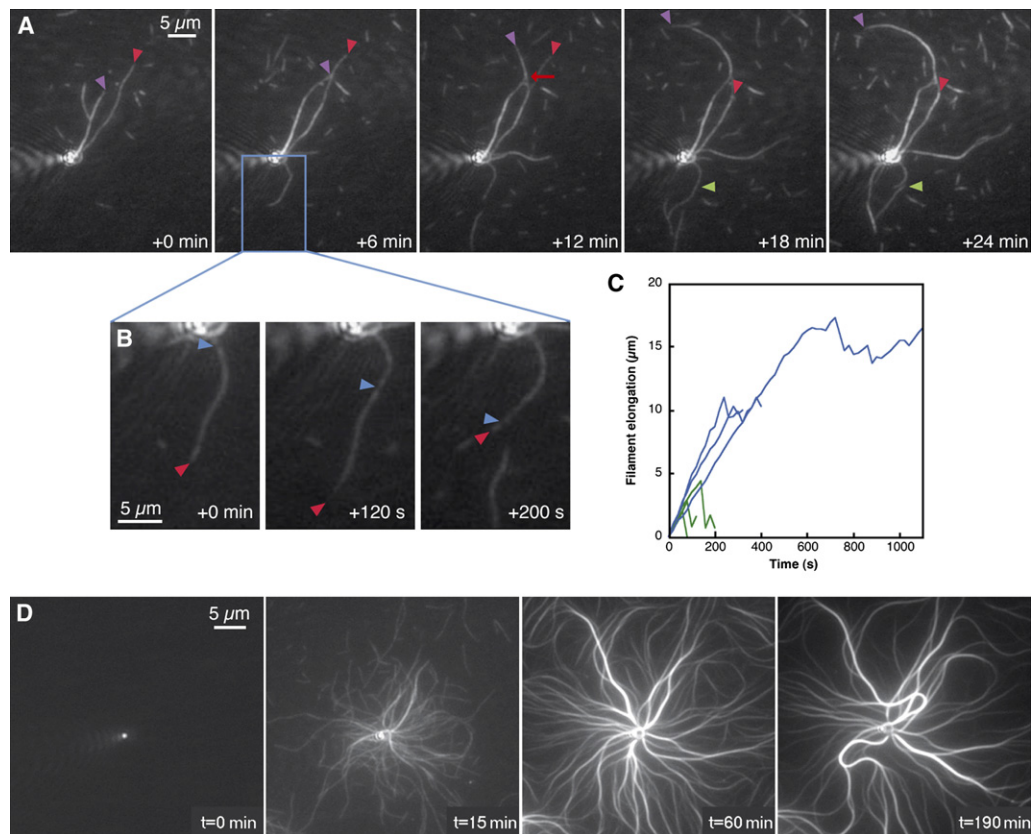
Figure 4. TIRF Microscopy Allows for the Visualization of Actin-Filament-Cable Formation and Explains the Symmetry Breaking in a mDia1-Based Motility Assay

Conditions: mDia1-coated beads were attached to the cover glass before the addition of 1.2 µM rhodamine-labeled actin monomers in the presence of 3.6 µM profilin and variable amounts of human cofilin.

(A) Time-lapse evanescent-wave microscopy of rhodamine-labeled-actin polymerization around a 100 nM mDia1-coated bead in the presence of 1 µM human cofilin and 3.6 µM profilin. Human cofilin efficiently severed (green triangle) and reduced the length of single actin filaments while they elongated (red triangle), whereas zippering of actin filaments (red arrow) generated thicker actin-filament cables that were more resistant to ADF/cofilin (purple triangle). See also Movie S12.

(B) Speckles inside the growing filaments (blue triangle) allowed us to demonstrate that during shortening phases (red triangle tracks the pointed end of an actin filament) the addition of subunits at the barbed end continues at the same rate. See also Movie S12. This figure represents an enlargement of the region defined by the blue box in (A).

(C) Length variation of a single filament before and after a zippering event. A typical zippering event is marked with the red arrow in (A). An actin filament after zippering is more resistant to ADF/cofilin fragmentation (blue curves) than an isolated actin filament (green curves). This is illustrated by the average length of isolated or zippered actin filaments.

(D) Time-lapse evanescent-wave microscopy of rhodamine-labeled-actin polymerization around a 1 µM mDia1-coated bead in the presence of 4 µM human cofilin and 3.6 µM profilin. Human ADF/cofilin principally severed single actin filaments rather than actin cables, leading to the gradual symmetry breaking and formation of large actin cables after 1 hr. After 3 hr, continuous insertion of actin monomers between the barbed ends of actin filaments and formins attached to the bead produced enough force to buckle the cables. See also Movie S13.

now, only minor catastrophes have been reported for single actin filaments [15]. The addition of BeF$_3$, which is a strong inhibitor of ADF/cofilin binding and mimics the ADP-P$_i$ state of actin filaments [16], to the protein mixture prevents the stochastic behavior of actin filaments (Movie S9). ADF/cofilin contributes to the shortening of actin filaments by clipping off the aged ends of continuously growing actin filaments (Figure 3A, Movie S8; and Figure 4A, Movie S12, green arrows mark an example of severing). The apparent elongation rate of formin-bound actin filaments is then determined by the addition of actin monomers at the barbed end and massive subunit loss resulting from the severing of varying lengths of filament from the distal or pointed end. Speckles in the actin filament (Figure 4B, blue triangle) confirm that, during a shortening phase

(Figure 4B, red triangle), the addition of actin monomers continues at the barbed end at a similar rate. This suggests that in the presence of formin, profilin, and ADF/cofilin the net polymerization at the growing barbed ends attached to a processive formin of 41.8 subunits per second is balanced by the subunit loss that results from ADF/cofilin trimming the aged end of the growing actin filament (Figures 3A and 4A; Movies S8 and S12).

By incorporating into our kinetic model all reactions that contribute to the effects of ADF/cofilin on actin dynamics (these reactions include binding to actin monomers and filaments, fragmentation, depolymerization, and an increase in the rate of phosphate dissociation from actin filaments), we were able to reproduce the two phases (i.e., elongation and shortening) of single actin filaments at the surface of formin-coated beads

(Figure 3B; Movie S10). Similar to our experimental con-
clusions, the kinetic simulation suggests that fragmen-
tation is the mechanism that counterbalances rapid
actin-filament elongation in the presence of formin.
Analysis of the variation in the length of actin filaments
attached to the beads by a processive formin, both ex-
perimentally (Figures 3A and 3C, red curve) and in silico
(Figures 3B and 3C, dashed blue curve), revealed that
after a rapid phase of elongation (about 100 s), a single
actin filament fluctuates rapidly between phases of
elongation and shortening. To compare experimental
and simulated data, we reduced the in silico number of
time points for the acquisition of actin-filament length
(Figure 3C, solid blue curve). We obtained similar pro-
files for the simulated and experimental dynamics of sin-
gle actin filaments with close average lengths (Figure 3C,
compare solid red and blue curves). These results sug-
gest that the fluctuations in the length of actin filaments
in our TIRFM experiment were probably underestimated
because of the limit of resolution of the microscope sys-
tem (i.e., 0.5 μm) and the time of acquisition between
consecutive frames; this acquisition time might have al-
lowed actin filaments to be severed and disappear from
the evanescent field between frames. The kinetic simu-
lation enabled us to predict that an actin subunit spends,
in our experimental conditions (Figure 3A; Movie S8), on
average, about 43 s on a growing actin filament before
dissociation by severing (Figure 3D; Movie S11). In-
creasing the concentration of ADF/cofilin reduces this
average time to a lower limit of 25 s, both experimentally
and in silico (Figure 3E).

Bundling Stabilizes Actin Filaments and Prevents ADF/Cofilin Severing

Although ADF/cofilin severs single actin filaments
quickly, we report here that higher-order structures
such as actin bundles were more resistant to ADF/cofilin
severing (Figures 4A and C; Movie S12). This is also ob-
served for actin-filament bundles generated by villin,
a crosslinking protein [17]. As the density of actin fila-
ments increased around the polystyrene beads, individ-
ual actin filaments started to interact with each other
through a "zippering" mechanism and generated actin-
filament bundles (Figure 4A, red arrow, 6 min; Movie
S12; and [13]). A comparison of the fluctuations in the
length of a single actin filament alone before (Figure 4C,
green curves) and after (Figure 4C, blue curves) a zipper-
ing event revealed an obvious increase in the persistence
of the elongation because of bundle formation. This
demonstrates that bundles were stabilized against frag-
mentation by ADF/cofilin, whereas surrounding single
actin filaments attached to the beads were still continu-
ously fragmented by ADF/cofilin (Figure 4A and Movie
S12, green arrows).

Zippering of Actin Filaments Inhibits ADF/Cofilin Activity and Favors the Formation of Large Actin Cables Responsible for Actin-Based Motility

The combination of TIRFM and a biomimetic system of
formin-coated polystyrene beads allowed us to deter-
mine the sequence of events leading from stationary
to motile beads (Figure 4D). Because actin, profilin,
and ADF/cofilin are the only proteins required in our mo-
tility assay, experiments were conducted with densely

coated beads (i.e., 1 μM mDia) in the presence of rhoda-
mine-actin, profilin, and human cofilin (Figure 4D; Movie
S13). After the addition of the protein mixture into the
flow cell, actin-filament polymerization began rapidly
around the beads (Figure 4D, 0 to 15 min; Movie S13).
Subsequently, it appeared that the dense mDia1 coat-
ing of the beads induced a saturation of the bead by ac-
tin filaments that contact each other because of thermal
fluctuations and then zipper to form large actin-filament
cables (Figure 4D, 15 to 60 min; Movie S13). Because
actin-filament cables became progressively stiffer and
brighter, we suggest that fragmentation by ADF/cofilin
is less efficient on these structures (Figure 4D, 60 to
190 min; Movie S13). After 1 hr, large actin bundles
were the predominant actin-based structures associ-
ated with the bead (Figure 4D; Movie S13). Two of these
cables started to buckle at a rate of elongation of
0.2 μm $\cdot$ min^{-1} (Figure 4D, 190 min; Movie S13), similar
to that of the large actin cables observed during the mo-
tility of the mDia1 bead (Figure 1). No motility was
observed in the TIRFM experiments, however, because
the nonspecific interaction of the beads with the cover
glass was required for maintaining the bead in the field
of the evanescent wave. In the absence of ADF/cofilin,
actin-filament bundles were organized randomly around
the beads (Movie S14).

We propose that, in the case of mDia1-coated beads,
the symmetry breaking that allowed motility (Figure 1)
was essentially due to the modulation of ADF/cofilin
severing efficiency by the actin-filament zippering that
drives large actin-filament cable formation (Figure 4D;
Movie S13). To further test this hypothesis, we used
a model (Figure S3) where we included the possibility
for actin filaments in close contact with each other to
produce cables that are resistant to ADF/cofilin sever-
ing (Movie S15). The interaction of ADF/cofilin with actin
filaments within bundles is modulated by the filament
accessibility and the change of the mechanical proper-
ties of bundles. We assumed that the affinity of ADF/
cofilin for actin filaments, K(N), depends on N, where
N is the number of actin filaments in the bundle [see
Supplemental Data for a discussion of K(N)]. This as-
sumption leads to a simulation consistent with the ex-
perimental data, in the sense that two large actin cables
positioned 180° from each other emanate from the bead
(Movie S15).

Discussion

Molecular Mechanism for Rapid Actin-Filament Turnover

The use of TIRFM provided unique insights into the
mechanism of actin polymerization initiated by the
FH1-FH2 domains of mDia1 at the surface of polystyrene
beads. We first resolved the controversial role of profilin
during the processive mechanism of actin-filament as-
sembly by formin [11, 14]. Profilin increased by 5-fold
the rate of addition of actin subunits at the barbed end
of an actin filament attached to mDia1; however, profilin
was not required for the processive behavior of mDia1,
in agreement with Kovar et al. (Movies S5–S6; and
[14]). The presence of ADF/cofilin in our reconstituted
system caused dramatic changes in the dynamic
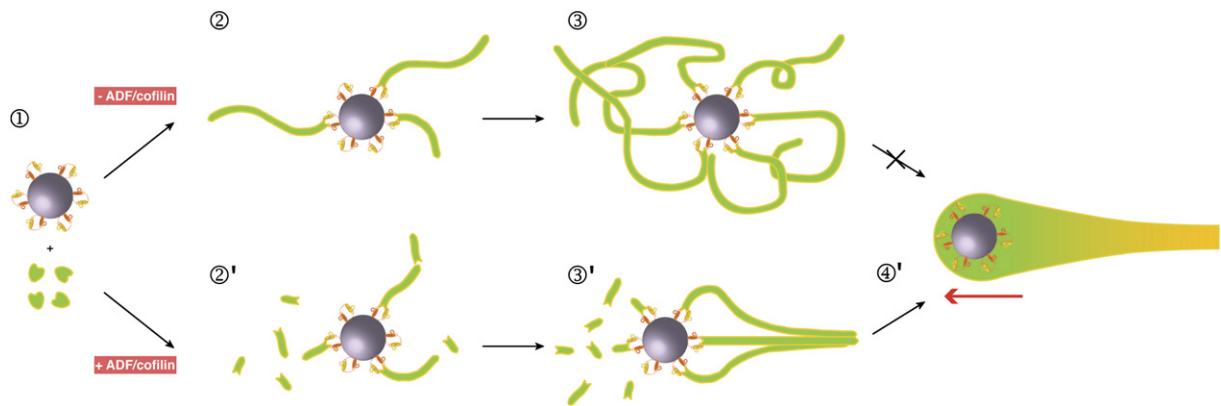
Figure 5. Model for the Link between Rapid Actin-Filament Turnover, Actin-Cable Formation, and Symmetry Breaking Prior to Actin-Based Force Generation

In the absence of ADF/cofilin, formin-coated beads are able to initiate actin filaments (step 1) that grow continuously and randomly around the beads (step 2). This generates a cloud of actin filaments around the beads (step 3). In the presence of ADF/cofilin, actin filaments initiated at the surface of the beads grow and shrink rapidly (step 2′). Lateral contact between actin filaments favors actin-bundle formation and enhances their stability against ADF/cofilin (step 3′). This selection process is the basis for symmetry breaking and actin force generation (step 4′).

behavior of individual actin filaments. We report here, for the first time, that single actin filaments can grow and shorten stochastically because ADF/cofilin clips the aged ends of continuously growing actin filaments.

In actin filaments attached to the beads by mDia1, the apparent rate of subunit loss due to ADF/cofilin severing can increase to values more than 35 s^{-1}, in the case of actin-filament shortening. A simple kinetic model constrained by experimental rate constants allowed us to reproduce qualitatively and quantitatively the type of stochastic dynamics that drives growing actin-filament turnover attached to a processive nucleator. Our kinetic model predicts that an actin subunit spends, in our experimental conditions, on average about 43 s on these actin filaments before release. This value is similar to the actin-filament turnover observed in vivo in fibroblasts [3], fish keratocytes [4], and yeast actin cables [18, 19]. The fragmentation or severing of growing actin filaments by ADF/cofilin is obviously the main property affecting actin-filament turnover. Severing has been reported previously but only on prepolymerized actin filaments (most likely in the ADP state) [20–23]. Here we observed for the first time the severing of growing filaments in real time. We predict that severing is modulated by the nucleotide status of subunits as they age along the length of a filament. To be efficient, this highly dynamic system needs to spatially separate zones of polymerization and fragmentation. The nucleotide state of actin filaments—ATP, ADP-P$_i$, or ADP—is then absolutely required as a timer controlling the efficiency of ADF/cofilin [16] and limits the possible fragmentation of actin filaments near the origin of nucleation where actin filaments are most likely ATP loaded [24]. Indeed, the average subunit residence time on a growing actin filament in the presence of a large concentration of ADF/cofilin reaches a lower limit of 25 s, essentially because of the presence of ATP-actin subunits in the filament (Figure 3E). Moreover, stabilization of the ADP-P$_i$ state of actin filaments by addition of BeF$_3$ prevents the ADF/cofilin dynamizing effect (Movie S9).

Model for Actin-Cable, or Bundle, Formation by the Synergistic Effects of Formin, Profilin, and ADF/Cofilin

Formin was initially reported to generate actin cables in yeast [25, 26]. A careful observation of yeast actin cables revealed that they are highly dynamic structures [18]. However, the actin-filament dynamics reported here raise the question of how such large actin-based structures can be generated and stabilized against the dynamizing activity of ADF/cofilin. We revealed that the dynamics of a single actin filament are related to whether it is laterally associated with another actin filament (Figure 5). Indeed, actin filaments comprising cables are partially stabilized against ADF/cofilin-mediated severing. Whereas single actin filaments rapidly grow and shrink and maintain an almost constant length after the initial growth period (Figure 5, step 2′), actin filaments organized into longitudinal structures grow more rapidly than they shrink, on average, allowing actin-cable formation (Figure 5, step 3′). This phenomenon can be easily explained if we consider the mechanism of action of ADF/cofilin. To have efficient severing activity, this protein needs to bind the side of actin filaments. However, ADF/cofilin binding to actin filaments is extremely slow and probably limited by filament breathing because of thermal fluctuations [27]. We propose that the increased mechanical rigidity of actin-filament bundles in comparison to that of isolated actin filaments [28] partially suppresses the filament breathing that is necessary for ADF/cofilin to bind efficiently. In addition, actin filaments inside a large actin-based structure, such as a bundle, are potentially less accessible to ADF/cofilin. Moreover, the severing of a bundle would require the simultaneous fragmentation of all actin filaments at the same location in the bundle, which must be an infrequent event. By growing rapidly, actin filaments generated close together by formin can associate laterally before destruction by ADF/cofilin (Figure 5, step 3′). This is a remarkable system because the actin-based structure controls its own stability.

Relationship between Actin-Cable Stability and Symmetry Breaking during Actin-Based Motility

Actin bundles generated at the surface of mDia1-coated beads are able to generate enough force to propel the bead (Figure 5, step 4′). However, mDia1 is most likely coated uniformly around a bead, and in the absence of ADF/cofilin, early polymerization events generate a symmetrical actin filament "cloud" (Figure 5, steps 2 and 3). We propose that the symmetry breaking necessary for bead motility is directly linked to the cooperative effect of the actin-filament zippering necessary for actin-cable formation and the related consequences to actin-filament stability against ADF/cofilin-mediated severing (Figure 5, steps 2′–4′). The process of initiating these large actin cables is relatively slow because at the beginning, thin bundles do not have an appreciable survival advantage with respect to ADF/cofilin severing and they frequently undergo catastrophic length reductions similar to those of single actin filaments. The symmetry-breaking phase begins when these bundles fuse together to form stiffer and larger structures. At this stage, both experimental data and simulations show that these bundles are strongly stabilized against ADF/cofilin, and the only noticeable change comes from the reduction of the population of bundles to two to four cables evenly distributed around the bead. Our experimental and in silico approaches do not include any crosslinking between filaments by specific proteins, such as fascin, villin, fimbrin, and α-actinin. In the presence of these actin-binding proteins, we predict that the resulting bundles would be stiffer and, as a consequence, would affect the process of cable formation by selection. The whole selection process is a simple and robust way to account for the emergence of the actin-based structures necessary for the production of forces of sufficient magnitude to drive beads or any other subcellular structure or membrane.

Experimental Procedures

Protein Expression and Production

Actin was isolated from rabbit-skeletal-muscle acetone powder [29]. Monomeric Ca-ATP-actin was purified by gel-filtration chromatography on Sephacryl S-300 [30] at 4°C in G buffer (5 mM Tris-HCl [pH 8.0], 0.2 mM ATP, 0.1 mM CaCl$_2$, and 0.5 mM DTT). Actin was labeled on Cys-374 to a stoichiometry of 0.8–1.0 with pyrene iodoacetamide ([31]; as modified by Pollard [32]) or on lysines with rhodamine or Alexa-532, according to Isambert et al. [33]. MgATP actin was prepared by incubation of Ca-ATP-actin on ice with 0.2 mM EGTA and an 11-fold molar excess of MgCl$_2$ over actin and used within 1 hr. Actin was polymerized by addition of one-tenth volume of 10× KMEI (500 mM KCl, 10 mM MgCl$_2$, 10 mM EGTA, and 100 mM imidazole-HCl [pH 7.0]). Profilin [34], Formin mDia1, FH1-FH2 domain [35], and human ADF/cofilin [36] were purified as described.

Coating of Beads

Carboxylated polystyrene microspheres (2 μm, Polyscience, Eppelheim, Germany) were coated with the indicated concentration of mDia1 FH1-FH2 according to Romero et al. [11].

Motility Assay

Beads were mixed with a motility medium containing 8 μM F-actin, 4 μM profilin, and 10 μM human cofilin in X buffer (10 mM HEPES [pH 7.8], 0.1 M KCl, 1 mM MgCl$_2$, 1 mM ATP, and 0.1 mM CaCl$_2$), supplemented with 1% BSA, 0.2% methylcellulose, 3 mM DTT, 1.8 mM ATP, and 0.1 mM DABCO. Image acquisition was performed on a Zeiss Axioplan microscope (Jena, Germany) equipped with a 63×/1.5 Plan-APOCHROMAT objective lens, and images were collected with a Hamamatsu ORCA CCD camera (Hamamatsu Photonics Deutschland GmbH) with Metavue version 6.2r6 (Universal Imaging, Media, PA).

Total-Internal-Reflection-Fluorescence-Microscopy

Glass flow cells were cleaned and prepared according to Kovar et al. [12]. Rhodamine-actin and Alexa-532-labeled actin-filament polymerization was observed and acquired as specified by Michelot et al. [13]. All data were analyzed with MetaMorph version 6.3r7 and plotted with Kaleidagraph v4.01 software (Synergy Software, Reading, PA).

Data Analysis

Elongation rates were determined by the measurement of filament lengths with MetaMorph version 6.2r6 during actin-filament elongation. Linear fits were made to the plots of length over time; the slopes represented elongation rates. Rates were converted from $\mu m \cdot s^{-1}$ to $\mu M^{-1} \cdot s^{-1}$ through the use of 333 actin monomers per micrometer [9]. All plots and fits were realized with Kaleidagraph v3.6 software.

Model of Actin-Filament Dynamics

We adapted the Gillespie algorithm to simulate the polymerization of actin filaments in a reaction-diffusion system (see Supplemental Data). The model for the zippering of filaments into bundles, as well as filament or bundle severing by ADF/cofilin, is discussed in the Supplemental Data section.

Supplemental Data

Experimental Procedures, three figures, one table, and fifteen movies are available at http://www.current-biology.com/cgi/content/full/17/10/825/DC1/.

References

1. Pollard, T.D., and Borisy, G.G. (2003). Cellular motility driven by assembly and disassembly of actin filaments. Cell 112, 453–465.
2. Mogilner, A. (2006). On the edge: Modeling protrusion. Curr. Opin. Cell Biol. 18, 32–39.
3. Wang, Y. (1985). Exchange of actin subunits at the leading edge of living fibroblasts: Possible role of treadmilling. J. Cell Biol. 101, 597–602.
4. Theriot, J.A., and Mitchison, T.J. (1991). Actin microfilament dynamics in locomoting cells. Nature 352, 126–131.
5. Medeiros, N.A., Burnette, D.T., and Forscher, P. (2006). Myosin II functions in actin-bundle turnover in neuronal growth cones. Nat. Cell Biol. 8, 215–226.
6. Schirenbeck, A., Bretschneider, T., Arasada, R., Schleicher, M., and Faix, J. (2005). The Diaphanous-related formin dDia2 is required for the formation and maintenance of filopodia. Nat. Cell Biol. 7, 619–625.
7. Moseley, J.B., and Goode, B.L. (2006). The yeast actin cytoskeleton: From cellular function to biochemical mechanism. Microbiol. Mol. Biol. Rev. 70, 605–645.
8. Pollard, T.D. (1986). Rate constants for the reactions of ATP- and ADP-actin with the ends of actin filaments. J. Cell Biol. 103, 2747–2754.

9. Pollard, T.D., Blanchoin, L., and Mullins, R.D. (2000). Molecular mechanisms controlling actin filament dynamics in nonmuscle cells. Annu. Rev. Biophys. Biomol. Struct. *29*, 545–576.

10. Loisel, T.P., Boujemaa, R., Pantaloni, D., and Carlier, M.F. (1999). Reconstitution of actin-based motility of *Listeria* and *Shigella* using pure proteins. Nature *401*, 613–616.

11. Romero, S., Le Clainche, C., Didry, D., Egile, C., Pantaloni, D., and Carlier, M.F. (2004). Formin is a processive motor that requires profilin to accelerate actin assembly and associated ATP hydrolysis. Cell *119*, 419–429.

12. Kovar, D.R., and Pollard, T.D. (2004). Insertional assembly of actin filament barbed ends in association with formins produces piconewton forces. Proc. Natl. Acad. Sci. USA *101*, 14725–14730.

13. Michelot, A., Derivery, E., Paterski-Boujemaa, R., Guerin, C., Huang, S., Parcy, F., Staiger, C.J., and Blanchoin, L. (2006). A novel mechanism for the formation of actin-filament bundles by a nonprocessive formin. Curr. Biol. *16*, 1924–1930.

14. Kovar, D.R., Harris, E.S., Mahaffy, R., Higgs, H.N., and Pollard, T.D. (2006). Control of the assembly of ATP- and ADP-actin by formins and profilin. Cell *124*, 423–435.

15. Fujiwara, I., Takahashi, S., Tadakuma, H., Funatsu, T., and Ishiwata, S. (2002). Microscopic analysis of polymerization dynamics with individual actin filaments. Nat. Cell Biol. *4*, 666–673.

16. Blanchoin, L., and Pollard, T.D. (1999). Mechanism of interaction of *Acanthamoeba* actophorin (ADF/cofilin) with actin filaments. J. Biol. Chem. *274*, 15538–15546.

17. Huang, S., Robinson, R.C., Gao, L.Y., Matsumoto, T., Brunet, A., Blanchoin, L., and Staiger, C.J. (2005). Arabidopsis VILLIN1 generates actin filament cables that are resistant to depolymerization. Plant Cell *17*, 486–501.

18. Yang, H.C., and Pon, L.A. (2002). Actin cable dynamics in budding yeast. Proc. Natl. Acad. Sci. USA *99*, 751–756.

19. Martin, S.G., and Chang, F. (2006). Dynamics of the formin for3p in actin cable assembly. Curr. Biol. *16*, 1161–1170.

20. Ichetovkin, I., Han, J., Pang, K.M., Knecht, D.A., and Condeelis, J.S. (2000). Actin filaments are severed by both native and recombinant *Dictyostelium* cofilin but to different extents. Cell Motil. Cytoskeleton *45*, 293–306.

21. Andrianantoandro, E., and Pollard, T.D. (2006). Mechanism of actin filament turnover by severing and nucleation at different concentrations of ADF/cofilin. Mol. Cell *24*, 13–23.

22. Maciver, S.K., Zot, H.G., and Pollard, T.D. (1991). Characterization of actin filament severing by actophorin from *Acanthamoeba castellanii*. J. Cell Biol. *115*, 1611–1620.

23. Pavlov, D., Muhlrad, A., Cooper, J., Wear, M., and Reisler, E. (2007). Actin filament severing by cofilin. J. Mol. Biol. *365*, 1350–1358.

24. Svitkina, T.M., and Borisy, G.G. (1999). Arp2/3 complex and actin depolymerizing factor/cofilin in dendritic organization and treadmilling of actin filament array in lamellipodia. J. Cell Biol. *145*, 1009–1026.

25. Evangelista, M., Pruyne, D., Amberg, D.C., Boone, C., and Bretscher, A. (2002). Formins direct Arp2/3-independent actin filament assembly to polarize cell growth in yeast. Nat. Cell Biol. *4*, 260–269.

26. Sagot, I., Klee, S.K., and Pellman, D. (2002). Yeast formins regulate cell polarity by controlling the assembly of actin cables. Nat. Cell Biol. *4*, 42–50.

27. Cao, W., Goodarzi, J.P., and De La Cruz, E.M. (2006). Energetics and kinetics of cooperative cofilin-actin filament interactions. J. Mol. Biol. *361*, 257–267.

28. Mogilner, A., and Rubinstein, B. (2005). The physics of filopodial protrusion. Biophys. J. *89*, 782–795.

29. Spudich, J.A., and Watt, S. (1971). The regulation of rabbit skeletal muscle contraction. I. Biochemical studies of the interaction of the tropomyosin-troponin complex with actin and the proteolytic fragments of myosin. J. Biol. Chem. *246*, 4866–4871.

30. MacLean-Fletcher, S., and Pollard, T.D. (1980). Mechanism of action of cytochalasin B on actin. Cell *20*, 329–341.

31. Kouyama, T., and Mihashi, K. (1981). Fluorimetry study of N-(1-pyrenyl)iodoacetamide labelled F-actin. Eur. J. Biochem. *114*, 33–38.

32. Pollard, T.D. (1984). Polymerization of ADP-actin. J. Cell Biol. *99*, 769–777.

33. Isambert, H., Venier, P., Maggs, A.C., Fattoum, A., Kassab, R., Pantaloni, D., and Carlier, M.F. (1995). Flexibility of actin filaments derived from thermal fluctuations. Effect of bound nucleotide, phalloidin, and muscle regulatory proteins. J. Biol. Chem. *270*, 11437–11444.

34. Fedorov, A.A., Pollard, T.D., and Almo, S.C. (1994). Purification, characterization and crystallization of human platelet profilin expressed in *Escherichia coli*. J. Mol. Biol. *241*, 480–482.

35. Li, F., and Higgs, H.N. (2003). The mouse Formin mDia1 is a potent actin nucleation factor regulated by autoinhibition. Curr. Biol. *13*, 1335–1340.

36. Carlier, M.F., Laurent, V., Santolini, J., Melki, R., Didry, D., Xia, G.X., Hong, Y., Chua, N.H., and Pantaloni, D. (1997). Actin depolymerizing factor (ADF/cofilin) enhances the rate of filament turnover: Implication in actin-based motility. J. Cell Biol. *136*, 1307–1322.